Published in final edited form as:
Nature. 2007 November 29; 450(7170): 676–682. doi:10.1038/nature06308.

A Two Ca^{2+}-Sensor Model for Neurotransmitter Release in a Central Synapse

Jianyuan Sun[1,2,*], **Zhiping P. Pang**[1], **Dengkui Qin**[1], **Abigail T. Fahim**[3], **Roberto Adachi**[3], and **Thomas C. Südhof**[1,2,4,*]

[1]Department of Neuroscience, The University of Texas Southwestern Medical Center, Dallas, TX 75390, USA

[2]Department of Molecular Genetics, The University of Texas Southwestern Medical Center, Dallas, TX 75390, USA

[3]Department of Pulmonary Medicine, The University of Texas M.D. Anderson Cancer Center, Houston, TX 77030, USA

[4]Howard Hughes Medical Institute, The University of Texas Southwestern Medical Center, Dallas, TX 75390, USA

Abstract

Ca^{2+}-triggered synchronous neurotransmitter release is well described, but asynchronous release – in fact, its very existence – remains enigmatic. Here, we report a quantitative description of asynchronous neurotransmitter release in calyx of Held synapses. We show that deletion of synaptotagmin-2 in mice selectively abolishes synchronous release, allowing us to study pure asynchronous release in isolation. Using photolysis experiments of caged-Ca^{2+}, we demonstrate that asynchronous release displays a Ca^{2+}-cooperativity of ~2 with a Ca^{2+}-affinity of ~44 μM, in contrast to synchronous release which exhibits a Ca^{2+}-cooperativity of ~5 with a Ca^{2+}-affinity of ~38 μM. Our results reveal that release triggered in wild-type synapses at low Ca^{2+}-concentrations is physiologically asynchronous, and that asynchronous release completely empties the readily-releasable pool of vesicles during sustained elevations in Ca^{2+}. We propose a two Ca^{2+}-sensor model of release that quantitatively describes the contributions of synchronous and asynchronous release under different presynaptic Ca^{2+}-dynamics conditions.

List of key genes/proteins

synaptotagmin; SNARE proteins; Ca^{2+}-channel

Two modes of Ca^{2+}-triggered neurotransmitter release were described. Fast synchronous release predominates in all synapses during low-frequency action-potential firing[1,2]. Slower asynchronous release mediates synaptic transmission in some synapses during high-frequency action-potential trains[3–7], but remains a minor component in other synapses[1,2]. Precise measurements of Ca^{2+}-triggering of synchronous release were obtained in the calyx

*To whom correspondence should be addressed (J.S., Jianyuan.Sun@UTSouthwestern.edu; T.C.S., Thomas.Sudhof@UTSouthwestern.edu).

Author contributions

J.S. performed the electrophysiology and photolysis experiments and modeling. Z.P.P. carried out the biochemical, immunohisochemical, and mouse genetics experiments; D.Q participated in the electrophysiology and photolysis experiments; A.T.F. and R.A. generated the synaptotagmin-2 KO mice, and T.C.S. and J.S. designed the experiments and wrote the manuscript.

Supplementary Information is linked to the online version of the paper at www.nature.com/nature.

of Held synapse that allows simultaneous patching of pre- and postsynaptic neurons, and enables monitoring of Ca^{2+}-currents and capacitance of nerve terminals[8–12]. Such measurements revealed that the Ca^{2+}-sensor for synchronous release exhibits an apparent cooperativity of ~5, and an apparent K_d of ~10 or ~105 μM Ca^{2+} (refs. 11 and 12). In vertebrate synapses, synaptotagmin-1, -2, and -9 function as Ca^{2+}-sensors for fast synchronous release[13–18], and exhibit a binding stoichiometry of 5 Ca^{2+}-ions/molecule and a micromolar Ca^{2+}-affinity. Of these synaptotagmins, synaptotagmin-2 is a likely Ca^{2+}-sensor for synchronous release at the calyx synapse because a mutation that decreases synaptotagmin-2 levels impairs synchronous release from calyx terminals[19].

In synapses with predominantly asynchronous release during high-frequency action-potential trains, asynchronous release out-competes synchronous release during the action-potential train[3–7]. Measurements of asynchronous release suggested a higher apparent Ca^{2+}-affinity, but the same Ca^{2+}-cooperativity as synchronous release[20,21]. These properties would explain the ability of asynchronous release to outcompete synchronous release during high-frequency action-potential trains because the accumulating residual Ca^{2+} in the train would trigger asynchronous release in the intervals between action potentials at Ca^{2+}-levels at which synchronous release cannot be induced. Consistent with this notion, Ca^{2+}-chelators such as EGTA block asynchronous release during high-frequency action potential trains but have less effect on synchronous release[3–6,22]. According to this view, synapses without predominantly asynchronous release during high-frequency trains, such as the calyx synapse, either lack asynchronous release, or have efficient Ca^{2+}-buffering and Ca^{2+}-extrusion mechanisms that prevent accumulation of residual Ca^{2+} (refs. 23 and 24). Moreover, the similar apparent Ca^{2+}-cooperativity of synchronous and asynchronous release suggested that asynchronous release could be a modification of synchronous release[25], indicating that there are no separate universal synchronous and asynchronous release pathways[24]. Indeed, quantitative models of release based on the assumption of a single Ca^{2+}-sensor are widely applicable[11,12]. These models, however, are inaccurate at low Ca^{2+}-concentrations; even a recently refined model that proposes an allosterically modulated release machinery with a single Ca^{2+}-sensor is unable to accurately predict release rates at low Ca^{2+}-concentrations[25]. Thus at present, no accurate quantitative model for neurotransmitter release is available. Evaluating asynchronous release and generating an accurate quantitative model for release is difficult because asynchronous release has primarily been characterized in synapses that have a strong synchronous component which could have contaminated the measurements[20,21], and because the biophysical properties of asynchronous release remain unknown. However, these questions have wide implications for our understanding of synaptic transmission because an accurate description of asynchronous release is required for any quantitative model of synaptic transmission. We now provide such a description in the calyx of Held synapse, and demonstrate that asynchronous release represents a separate and distinct release pathway that is likely to be universally present in synapses.

Synaptotagmin-2 KO blocks synchronous release

Mice lacking synaptotagmin-2 initially develop normally, but perish after postnatal day 21 (P21). In the calyx of Held, we detected no co-expression of synaptotagmin-1 with synaptotagmin-2 at any time between P5 and P14, or of synaptotagmin-9 at P11 (Fig. 1a; Suppl. Fig. 2). Moreover, we observed no compensatory increases of synaptotagmin-1 in synaptotagmin-2 deficient calyces, and found no overall change in protein composition (Fig. 1b and Suppl. Figs. 2–4). Thus, calyx terminals express only one (synaptotagmin-2) of the three synaptotagmins that serve as Ca^{2+}-sensors for synchronous release[18,19], presumably because synaptotagmin-2 is the fastest Ca^{2+}-sensor[18] and the calyx synapse is specialized for precise fast responses[8,9].

To determine the effect of the synaptotagmin-2 deletion on release, we examined brainstem slices from 7–9 day-old mice. Using cell-attached patches on presynaptic calyx terminals, we induced a train of presynaptic action potentials, and measured postsynaptic responses by whole-cell recordings. Strikingly, evoked synaptic responses in synaptotagmin-2 deficient terminals were small and delayed, with release being increasingly triggered in the inter-stimulus intervals during the stimulus train (Fig. 1c). These responses are consistent with the notion that in the absence of synaptotagmin-2 as the Ca^{2+}-sensor for synchronous release, accumulating Ca^{2+} during the stimulus train triggers asynchronous release.

To characterize this release, we induced presynaptic action potentials by afferent fiber stimulations, and recorded EPSCs at different extracellular Ca^{2+}-concentrations ($[Ca^{2+}]_e$ = 0.3–10 mM). At 0.3–0.7 mM $[Ca^{2+}]_e$, wild-type and mutant terminals exhibited similar amounts of release (Figs. 2a and 2b). At 2 mM and 10 mM $[Ca^{2+}]_e$, however, synaptotagmin-2 deficient terminals displayed >10-fold smaller EPSC amplitudes and charge transfers than wild-type terminals (Figs. 2a and 2b). Moreover, at 2 mM $[Ca^{2+}]_e$ (a nearly physiological concentration), synaptotagmin-2 deficient synapses were ~3-times slower in reaching the EPSC maximum (Fig. 2c), and exhibited a ~5-fold slower release kinetics (measured as the time to achieve 50% synaptic charge transfer; wild-type (WT) = 4.9±0.7 ms; synaptotagmin-2 knockout (KO) = 26.8±1.7 ms; $p<0.01$; Suppl. Fig. 5). We conclude that deletion of synaptotagmin-2 severely impairs fast synchronous release in the calyx of Held synapse but leaves a slower, asynchronous form of Ca^{2+}-triggered release intact. In addition, the deletion of synaptotagmin-2, like that of synaptotagmin-1 in forebrain[19], increased the frequency of miniature spontaneous release events but did not alter the size and kinetics of these events (Suppl. Fig. 6).

A potential concern is that since the synaptotagmin-2 KO mice die at P21-P24, the KO neurons may not be healthy. However, at P9-P14 when we analyze the synaptotagmin-2 KO mice, the KO mice are not visibly distressed, the protein composition of their brainstems is not detectably altered (Suppl. Fig. 4), and the basic electrical properties of the postsynaptic calyx neurons are not impaired (Suppl. Table 1). Thus, the changes we observe in the KO mice are likely specifically caused by the deletion of synaptotagmin-2.

Ca^{2+}-currents and readily-releasable pool size

In presynaptic terminals of the calyx of Held, action potentials gate Ca^{2+}-influx via P/Q- and N-type Ca^{2+}-channels[26,27]. Since synaptotagmin-1 interacts with Ca^{2+}-channels[28–30], we tested whether deletion of the highly homologous synaptotagmin-2 impairs Ca^{2+}-channel function. We simultaneously patched presynaptic calyx terminals and postsynaptic neurons in the presence of drugs that block action-potential propagation, AMPA-receptor desensitization, and NMDA-receptor activation. We then recorded presynaptic Ca^{2+}-currents and postsynaptic EPSCs in response to prolonged depolarization (4 ms predepolarization from −80 to +80 mV followed by 50 ms depolarization to +20 mV)[31]. Deletion of synaptotagmin-2 caused no detectable change in the amplitudes of presynaptic Ca^{2+}-currents, electrical charge transfer mediated by the Ca^{2+}-channels (integrated over 100 ms), or their I/V relationship, suggesting that synaptotagmin-2 is not involved in regulating Ca^{2+}-channels (Figs. 3a–3c, and Suppl. Figs. 7 and 8).

The 50 ms depolarization in Fig. 3a depletes the readily-releasable pool (RRP) of vesicles by inducing a prolonged increase in intracellular $[Ca^{2+}]_i$ (ref. 31). Postsynaptic recordings of synaptic responses showed that deletion of synaptotagmin-2 depressed the peak amplitude of the depolarization-induced EPSC ~2-fold, slowed its risetime ~3-fold, and increased its latency ~5-fold (Figs. 3d–3f). However, the synaptotagmin-2 deletion did not alter the total synaptic charge transfer induced by the 50 ms presynaptic depolarization (Fig. 3g; integrated

over 2 s). Thus, deletion of synaptotagmin-2 did not affect the size of the RRP, and asynchronous release induces exocytosis of the entire RRP of vesicles in the absence of synaptotagmin-2, albeit with a slower timecourse.

To compare the size of the RRP in wild-type and KO mice by an independent approach, we puffed a 2 M sucrose solution onto the terminal for 1 s, and integrated the synaptic charge transfer of the induced EPSCs over 2 s (Figs. 3h and 3i, Suppl. Fig. 9). Again, no difference between wild-type and synaptotagmin-2 deficient terminals was detected. The absolute size of the RRP determined after sustained depolarization was larger than the RRP size measured by puffing of hypertonic sucrose (Fig. 3). This difference may be due to the distinct measurement conditions used (ESPCs induced by depolarization but not by sucrose were monitored in the presence of cyclothiazide as a blocker of receptor desensitization); in addition, Ca^{2+}-dependent mobilization of the RRP during the depolarization may have increased its size during the monitoring period[32].

Ca^{2+}-dependence of release

To characterize the Ca^{2+}-dependence of transmitter release at wild-type and synaptotagmin-2 deficient synapses, we determined the peak release rates in calyx terminals as a function of the presynaptic intracellular Ca^{2+}-concentration $[Ca^{2+}]_i$. For Ca^{2+}-concentrations of <1 μM, we employed two methods: injection of terminals via the patch pipette with defined concentrations of Ca^{2+} and Ca^{2+}-buffers, or with caged Ca^{2+} (9 mM DM-nitrophen, 8.6 mM $CaCl_2$, and various Ca^{2+}-buffers) that is released by flash photolysis with a weak laser pulse (Suppl. Fig. 10)[11,12,33,34]. For Ca^{2+}-concentrations >1 μM, we employed only the flash photolysis method with a stronger laser pulse. Flash photolysis of caged Ca^{2+} produces a rapid and spatially uniform, defined rise in $[Ca^{2+}]_i$ that we monitored *in situ* in the terminals using co-injected Ca^{2+}-indicator dyes. In order to cover the entire range of Ca^{2+}-concentrations examined (0.1–15 μM), we employed three different Ca^{2+}-indicator dyes (Fura2, Fura-4F, and Fura-6F), and calibrated the Ca^{2+}-signals directly in the calyx terminals (Suppl. Fig. 10). Finally, we quantified vesicle exocytosis by deconvolution of evoked EPSCs, using a measured miniature EPSC waveform to calculate the release rates[31] (see Methods and Suppl. Materials).

We first elevated $[Ca^{2+}]_i$ to concentrations of 0.05–1.0 μM. Increases of $[Ca^{2+}]_i$ to <0.2 μM induced an enhancement in mEPSC frequency but no clearcut evoked EPSCs (Fig. 4a). At these Ca^{2+}-concentrations, release was slightly higher in synaptotagmin-2 deficient than in wild-type synapses (Fig. 4e), presumably because deletion of synaptotagmin-2 increases the resting frequency of mEPSCs (Suppl. Fig. 6). At $[Ca^{2+}]_i$ of 0.2–1.0 μM, wild-type and synaptotagmin-2 deficient synapses exhibited indistinguishable release rates, independent of whether the $[Ca^{2+}]_i$ was constantly clamped with Ca^{2+}-buffers, or acutely raised by photolysis of caged Ca^{2+} with a weak flash (Fig. 4 and Suppl. Fig. 11). Thus, as observed for action potential-induced release at low $[Ca^{2+}]_e$ (Fig. 2), deletion of synaptotagmin-2 does not impair release evoked at low $[Ca^{2+}]_i$. This result suggests that even in wild-type synapses, release at low $[Ca^{2+}]_i$ is physiologically mediated by the asynchronous Ca^{2+}-sensor, a conclusion that is consistent with previously described properties of release induced by low $[Ca^{2+}]_i$ (ref. 35).

We next examined larger increases in $[Ca^{2+}]_i$ produced by flash photolysis of caged Ca^{2+}. In wild-type neurons, a peak release rate of ~24 vesicles/ms was evoked when $[Ca^{2+}]_i$ was elevated to 2 μM (Fig. 4c). The peak release rate steeply increased to ~1750 vesicles/ms when $[Ca^{2+}]_i$ was raised to 9.2 μM, demonstrating a very high Ca^{2+}-cooperativity (Fig. 4d). In synaptotagmin-2 deficient synapses, conversely, a 2 μM $[Ca^{2+}]_i$ rise caused release with a

peak rate of 3.7 vesicle/ms. Elevation of $[Ca^{2+}]_i$ to 10.5 μM only increased the release rate to 31 vesicles/ms, revealing a much lower Ca^{2+}-cooperativity.

Figure 4e displays the Ca^{2+}-dependence of the peak release rate obtained from 78 wild-type (open symbols) and 106 synaptotagmin-2 deficient terminals (filled symbols), plotted on logarithmic coordinates (see Suppl. Table 2 for numerical values). Whereas at $[Ca^{2+}]_i$ of <1 μM, the vesicular release rates are not decreased in synaptotagmin-2 deficient terminals, at $[Ca^{2+}]_i$ of >2 μM, deletion of synaptotagmin-2 reduced the peak transmitter release rate 10–40 fold compared to wild-type synapses. In the most dynamic range of 0.7–5 μM $[Ca^{2+}]_i$, the relation of the peak release rate to $[Ca^{2+}]_i$ follows a 5^{th} power function in wild-type terminals, but only a 2^{nd} power function in synaptotagmin-2 deficient terminals (Fig. 4e). At higher $[Ca^{2+}]_i$, release saturates in wild-type synapses, but not in KO synapses. Thus, whereas release triggered at $[Ca^{2+}]_i$ of 0.2–1.0 μM exhibits a similarly low Ca^{2+}-cooperativity and magnitude in wild-type and synaptotagmin-2 deficient synapses, release triggered at >1 μM $[Ca^{2+}]_i$ exhibits a dramatically different Ca^{2+}-cooperativity and magnitude in wild-type and mutant synapses.

A potential concern with a genetic study is that a compensatory developmental change could lead to the expression of a non-physiological Ca^{2+}-sensor in mutant synapses. However, the fact that release at low $[Ca^{2+}]_i$, measured with $[Ca^{2+}]_i$ raised by two different methods, is indistinguishable between wild-type and synaptotagmin-2 deficient synapses argues strongly against such a developmental change in the mutant terminals because such a change should have affected the behavior of Ca^{2+}-triggered release at all Ca^{2+}-concentrations. Moreover, the good prediction of release in both wild-type and mutant synapses by our quantitative model described below is inconsistent with such a change.

A two Ca^{2+}-sensor model of release

Previous Ca^{2+}-photolysis studies on calyx synapses prompted formulation of a quantitative model of neurotransmitter release with a single Ca^{2+}-sensor for release (referred to here as 'conventional 1-sensor model')[11,12]. These models, however, were unable to predict release at low $[Ca^{2+}]_i$ (Figure 5a), presumably because this release – as depicted in Figures 2 and 4 – is primarily carried by the asynchronous Ca^{2+}-sensor. Partly to remedy this problem, and partly to account for the change in release induced by phorbol esters, an allosteric model of release was proposed[25] that improves prediction of the Ca^{2+}-dependence of peak release rates (Fig. 5a). The allosteric model, however, also postulates a single Ca^{2+}-sensor, and underestimates the time-to-peak rate at lower $[Ca^{2+}]_i$ (Fig. 5b). To formulate a more accurate model, we developed a two Ca^{2+}-sensor kinetic model based on the current information (Fig. 5c). This model postulates that (1) synchronous release is triggered by Ca^{2+}-binding to a Ca^{2+}-sensor with a Ca^{2+}-cooperativity of ~5 consistent with the Ca^{2+}-binding properties of synaptotagmins; (2) asynchronous release is triggered by Ca^{2+}-binding to an unidentified Ca^{2+}-sensor with a Ca^{2+}-cooperativity of ~2 (Fig. 4); and (3) spontaneous release occurs with an effectivity factor C to account for the change in spontaneous release in synaptotagmin-deficient synapses[17,19] (Suppl. Fig. 6). The two Ca^{2+}-sensor model assumes that these three release pathways compete with each other, and operate on the same vesicle pools.

The two Ca^{2+}-sensor model allows a satisfactory description of all of our Ca^{2+}-photolysis data, both for the Ca^{2+}-dependence of the peak release rates and of the time-to-peak rate for wild-type and synaptotagmin-2 deficient synapses (Figs. 5a and 5b). Moreover, the two Ca^{2+}-sensor model accurately predicts the kinetics of Ca^{2+}-dependent vesicle release in wild-type and synaptotagmin-2 deficient calyx synapses (Figs. 5d and 5e and Suppl. Fig. 13). The two Ca^{2+}-sensor model calculates that synchronous release exhibits an apparent

Ca^{2+}-affinity of ~38 μM a Ca^{2+}-cooperativity of ~5, and an apparent k_{on} rate of α=1.53 10^8 $M^{-1}s^{-1}$, and that asynchronous release exhibits a similar apparent Ca^{2+}-affinity of ~44 μM, but a much lower Ca^{2+}-cooperativity of ~2, and a much slower k_{on} rate of χ=2.94 10^6 $M^{-1}s^{-1}$ (Fig. 5).

Our parameters for synchronous release are squarely in the middle between the two previous estimates in calyx synapses[11,12], but our parameters for asynchronous release differ from previous suggestions[20,21], probably because previous suggestions were based on extrapolations of asynchronous release in the continued presence of synchronous release that may have contaminated the estimates. Although the two Ca^{2+}-sensor model thus reveals that asynchronous release exhibits a relatively low apparent Ca^{2+}-affinity, the model still predicts that asynchronous release is the major physiological mode of synaptic transmission at low $[Ca^{2+}]_i$ because its lower degree of Ca^{2+}-cooperativity renders asynchronous release more effective at low $[Ca^{2+}]_i$. At high $[Ca^{2+}]_i$, conversely, synchronous release dominates because the predicted k_{on} for synchronous release is ~100-fold higher than that for asynchronous release (Fig. 5).

Summary

Here we show that among synaptotagmin isoforms that act as Ca^{2+}-sensors for synchronous release[18], calyx terminals only express synaptotagmin-2 (Fig. 1 and Suppl. Fig. 2). We demonstrate that in calyx terminals, synaptotagmin-2 is essential for Ca^{2+}-triggering of fast synchronous release (Fig. 2), but not for Ca^{2+}-influx or vesicle priming (Fig. 3). Thus, synaptotagmin-2 – as suggested for synaptotagmin-1 in forebrain synapses[13] – is selectively required for Ca^{2+}-triggering of fast release. We show that although asynchronous release contributes little to action potential-induced vesicle exocytosis in wild-type calyx synapses at physiological $[Ca^{2+}]_i$, asynchronous release triggers exocytosis of the entire RRP upon prolonged increases in $[Ca^{2+}]_i$ in synaptotagmin-2 KO calyx synapses (Fig. 3). Therefore, synchronous and asynchronous release act on the same vesicle pools. Moreover, release at low $[Ca^{2+}]_i$ exhibits a similar magnitude and Ca^{2+}-dependence in wild-type and synaptotagmin-2 deficient synapses, suggesting that release at low $[Ca^{2+}]_i$ is normally asynchronous, and that asynchronous release does not change in the KO mice.

Traditionally, asynchronous release is explained by three competing hypotheses: (1) Asynchronous and synchronous release share the same Ca^{2+}-sensor, but differ in the coupling of vesicles to Ca^{2+}-channels, the state of the vesicles, and/or the Ca^{2+}-buffering mechanisms involved[24,25,36,37]; (2) synchronous and asynchronous release are mediated by the same Ca^{2+}-sensor but utilize different, allosterically regulated vesicle pools[38]; and (3) different Ca^{2+}-sensors with distinct properties mediate synchronous and asynchronous release[13]. Clearly the distance between synaptic vesicles and Ca^{2+}-channels is a major determinant of the vesicular release probability, and differences in the Ca^{2+}-channel proximity of vesicles likely contribute to the vesicles' heterogeneity of release probabilities[39]. Moreover, undoubtedly different pools of vesicles exist and contribute to the heterogeneity of release probabilities at a synapse. Nevertheless, these differences are probably unrelated to the differences between synchronous and asynchronous release, but rather involved in regulating all release. Indeed, the following findings suggest that synchronous and asynchronous release are caused by independent mechanisms:

- Synchronous and asynchronous release exhibit qualitatively different properties, as evidenced by the unexpectedly low Ca^{2+}-affinity and distinctly low Ca^{2+}-cooperativity of asynchronous release, and by its persistence after synchronous release was selectively eliminated upon deletion of synaptotagmin-2 (Fig. 4).

- Asynchronous release is independent of the proximity of synaptic vesicles to Ca^{2+}-channels since our flash photolysis experiments produce a uniform increase in $[Ca^{2+}]_i$ that bypasses Ca^{2+}-channel activation (Fig. 4).
- Single Ca^{2+}-sensor models[11,12] adequately describe release at higher $[Ca^{2+}]_i$ but are unable to account for release at low $[Ca^{2+}]_i$. Even the sophisticated allosteric model[25] underestimates the time-to-peak release rate at low $[Ca^{2+}]_i$ (Fig. 5B).
- Release in wild-type and synaptotagmin-2 deficient terminals is identical at low $[Ca^{2+}]_i$ (Figs. 2 and 4), suggesting that this type of release is physiologically asynchronous. Moreover, asynchronous release becomes apparent during high-frequency action-potential trains in wild-type calyx synapses (Suppl. Fig. 14), consistent with studies of the precise kinetics of individual EPSCs demonstrating that asynchronous release in the calyx normally occurs even during isolated action protentials[40].

The definition of the biophysical properties of asynchronous, Ca^{2+}-triggered release made it possible to formulate a quantitative model for neurotransmitter release that likely applies to all synapses (Fig. 5). Our model indicates that the Ca^{2+}-sensors for synchronous and asynchronous release operate in competition with each other, with the asynchronous Ca^{2+}-sensor being slower but able to bind Ca^{2+} at lower concentrations, whereas the synchronous Ca^{2+}-sensor is faster with a higher Ca^{2+}-cooperativity. As a result, in this competition the synchronous Ca^{2+}-sensor 'wins' during pulses of high Ca^{2+}-concentrations, while the asynchronous Ca^{2+}-sensor prevails during sustained phases of lower Ca^{2+}-concentrations (Fig. 5). Within this framework, differences between synapses are primarily determined by which synaptotagmin isoform is being used as Ca^{2+}-sensor for synchronous release[18], and by the accumulation of residual Ca^{2+} in the intervals between action potentials during stimulus trains (i.e., by the Ca^{2+}-buffering properties)[34–36,41]. It is of interest here that fittingly, the calyx terminals with their exquisitely fast release properties use as synchronous Ca^{2+}-sensor only synaptotagmin-2, the fastest of the three Ca^{2+}-sensors for synchronous release.

METHODS SUMMARY

Synaptotagmin-2 KO mice were bred and genotyped as described[17]. Brain slices (200 μm) containing MNTB were prepared in a parasagital orientation from P7-P9 mice (for double patch or presynaptic cell-attached recording), or in a transverse orientation from P10-P14 mice (for fiber stimulation and purely post-synaptic recordings), and employed for single and/or double whole-cell recordings of nerve terminals and MNTB neurons with presynaptic electrical stimulation or stimulation by Ca^{2+}-uncaging or Ca^{2+}-dialysis largely as described[11,12,31,38,42]. Ca^{2+}-uncaging was achieved with an intense UV pulse from a frequency-tripled YAG-ND laser, and the resulting Ca^{2+}-concentrations were measured *in situ* by ratiometric fluorescence imaging of nerve terminals filled with fura-2, fura-4F, or fura-6F (Suppl. Fig. 10)[34,43]. Ca^{2+}-dyes were calibrated *in situ*. Release rates were calculated using the Neher deconvolution program (http://www.mpibpc.mpg.de/groups/neher/software/index.html) with a mEPSC size of 30 pA and a measured waveform[31]. We applied the different kinetic models to fit the data in our experiments (Figs. 5a–b and Suppl. Figs. 11 and 13). The conventional and the allosteric single Ca^{2+}-sensor kinetic models were simulated as described[11,12,25] (Suppl. Fig. 13). In our two Ca^{2+}-sensor model, each vesicle in the RRP can be released via three independent pathways (Fig. 5): 1) Ca^{2+}-independent fusion in the spontaneous mode, i.e. direct exocytosis of vesicles from the RRP with a release rate of $\gamma 1$. An effectivity factor (C) to account for the change in spontaneous release rate in synaptotagmin-1 and -2 deficient synapses was included; 2) Synchronous Ca^{2+}-evoked fusion mode triggered by full occupancy of the 5 binding sites of the synchronous

release Ca^{2+}-sensor[12,25]; 3) Asynchronous Ca^{2+}-evoked release triggered by occupancy of 2 Ca^{2+}-binding sites of an unidentified Ca^{2+}-sensor.

METHODS

Synaptotagmin-2 KO mice were bred and genotyped as described[17] (see Suppl. Materials for detailed methods). All analyses were performed on littermate offspring from heterozygous matings ("wild-type mice" = homo- or heterozygous for the wild-type allele).

Slice electrophysiology

Brain slices (200 μm) containing MNTB were prepared in a parasagital orientation from P7-P9 mice (for double patch or presynaptic cell-attached recording), or in a transverse orientation from P10-P14 mice (for fiber stimulation and purely post-synaptic recordings) were employed for single and/or double whole-cell recordings of nerve terminals and MNTB neurons largely as described[31,42]. All experiments involved postsynaptic whole-cell recordings with an Axopatch 200B amplifier (Axon Instruments Inc., CA). Presynaptic whole-cell recordings were obtained with an EPC-9 amplifier (HEKA, Lambrecht, Germany). The pre- and postsynaptic series resistances (<15 M′Ω and 7 M′Ω) were compensated by 60% and 98% (lag 10 μs), respectively. Both pre- and postsynaptic currents were low-pass filtered at 5 kHz and digitized at 20 kHz. Six recording configurations were employed (see Suppl. Materials for details):

a. Presynaptic cell-attached current injections to induce presynaptic action-potential trains with postsynaptic whole-cell recordings that monitor the evoked EPSCs (Fig. 1c). Stimulations were applied as 40 presynaptic current injections of 1 nA for 3 ms at 50 Hz.

b. Presynaptic afferent fiber stimulations with postsynaptic whole-cell voltage-clamp recordings (Fig. 2). Stimuli were applied with a bipolar electrode delivering 3–30 V for 0.1 ms.

c. Double-patch recordings by simultaneous pre- and postsynaptic whole-cell voltage-clamp recordings to measure the presynaptic RRP and Ca^{2+}-currents (Figs. 3a–3g). Stimulations consist of a presynaptic 4 ms predepolarization to 70–80 mV, followed by 50 ms depolarization to 20 mV.

d. Sucrose stimulation with postsynaptic whole-cell voltage clamp recordings to measure the RRP (Figs. 3h and 3i). Stimulation involves puffing 2 M sucrose in bath solution onto the target terminal with a pipette that is located about 5 μm from the calyx.

e. Double patch experiments for simultaneous measurements of presynaptic $[Ca^{2+}]_i$ and postsynaptic ESPCs with manipulation of the presynaptic $[Ca^{2+}]_i$ (Fig. 4). Stimulations were effected either by dialysis of Ca^{2+}-containing solutions into the terminal via the presynaptic pipette solution (Fig. 4e and Suppl. Figs. 11a and 11b), or by flash photolysis of DM-nitrophen/ Ca^{2+}(Fig. 4 and Suppl. Fig. 11c). Release rate was estimated by deconvolution[31].

f. Mini recordings (Suppl. Fig. 6 and Suppl. Methods).

All recordings were performed in the presence of 50 μM D-AP5 in the bath; in addition, for the double-patch experiments in c and e, we added 0.1 mM cyclothiazide and 1 mM kynurenic acid or 2 mM γ-DGG when strong flash photolysis was given resulting in $[Ca^{2+}]_i$ of >3 μM, in which case the obtained EPSCs were multiplied by 2 because control experiments determined that 2 mM γ-DGG decreased the EPSC amplitude 2-fold.

Ca^{2+}-uncaging and Ca^{2+}-imaging

The Ca^{2+}-uncaging and Ca^{2+}-imaging setup (Suppl. Fig. 5a) used an intense UV pulse from a frequency-tripled YAG-ND laser (355 nm, Surelite I, Continuum, CA) for Ca^{2+}-uncaging. Ca^{2+}-concentrations were measured *in situ* by ratiometric fluorescence imaging of nerve terminals filled with fura-2, fura-4F, or fura-6F (refs. 34,43). Ca^{2+}-indicator dyes were excited with a UV light source at 340 nm and 380 nm (energy ≤175W) using a monochromator (DG-4, Sutter Instrument, CA). The laser pulse was coupled into the epifuorescence port of an Axioskop and combined with the UV light using a beam-splitter (customized 90%T/10%R for 355 nm with a bandwith of <10 nm, Chroma Tech, VT). Both UV beams were collimated to optimize the intensity on the targeted terminal. A CCD camera (ORCA-ER, Hamamatzu, Japan) with on-chip binning was used to capture infrared images (300×300 pixels) and Ca^{2+}-images (19×19 pixels) of the terminal (Suppl. Figs. 9b and 9c). The fluorescence in the measuring area with background fluorescence subtraction (off-line) was used to calculate the $[Ca^{2+}]_i$. Images were captured using MetaFluor software and analyzed by IgorPro (Wavemetrics). For *in vivo* calibration of Ca^{2+}-indicator signals, we introduced Ca^{2+} indicators with an intracellular K-Gluconate pipette solution into the terminal (see Suppl. Materials). For fura-2 imaging, we used exposure times of 30 ms (in photolysis experiments) and 100 ms (for defined $[Ca^{2+}]$ solution injection experiment) with a 2 Hz capture rate. For fura-4F and fura-6F imaging, we used 10 ms exposure times with 2 Hz capture rates before the flash, and 10–30 Hz capture rates after the flash. Ca^{2+}-relaxation rates were modulated by the UV-illumination during the ratiometric Ca^{2+}-imaging procedure which was thus adjusted to maintain stable Ca^{2+}-levels (see Suppl. Materials).

Data processing and modeling

Release rates were calculated using the Neher deconvolution program (http://www.mpibpc.mpg.de/groups/neher/software/index.html) with a mEPSC size of 30 pA and a measured waveform[31].

Modeling

We applied the different kinetic models to fit the data in our experiments (Fig.5a–b). The conventional one Ca^{2+}-sensor kinetic model and the allosteric one Ca^{2+}-sensor kinetic model were simulated as described[11,12,25] (see Suppl. Fig. 13 legend). In our two Ca^{2+}-sensor model, each vesicle in the RRP can be released via three independent pathways: 1) Ca^{2+}-independent fusion in the spontaneous mode, i.e. direct exocytosis of vesicles from the RRP with a release rate of $\gamma 1$. An effectivity factor (C) to account for the change in spontaneous release rate in synaptotagmin-1 and -2 deficient synapses was included; 2) Synchronous Ca^{2+}-evoked fusion mode triggered by full occupancy of the 5 binding sites of the synchronous release Ca^{2+}-sensor[12,25]; 3) Asynchronous Ca^{2+}-evoked release triggered by occupancy of 2 Ca^{2+}-binding sites of an unidentified Ca^{2+}-sensor. The Ca^{2+} binding states can be defined by XnYm(t), where Xn represents the state in which n binding sites of the Ca^{2+}-sensor for synchronous release have been occupied (n=0–5), and Ym the state in which m binding sites of Ca^{2+} sensor of asynchronous release have been occupied (m=0–2). α and β represent the binding and dissociation constants, respectively, of the Ca^{2+}-sensor for synchronous release, and χ and δ the binding constants for asynchronous release, respectively. b is the cooperativity factor[34]. Note that $X0Y0|_{t=0}$=RRP. The kinetics of Ca^{2+}-binding states can be described as:

when 0<n<5,0<m<2:

$$d(XnYm)/dt = \alpha\cdot(5-n+1)\cdot Xn-1Ym\cdot[Ca^{2+}]_i + \beta\cdot b^n\cdot(n+1)\cdot Xn+1Ym - \alpha\cdot(5-n)\cdot XnYm\cdot[Ca^{2+}]_i - \beta\cdot b^{n-1}\cdot n\cdot XnYm + \chi\cdot(2-m+1)\cdot XnYm-1\cdot[Ca^{2+}]_i + \delta\cdot b^m\cdot(m+1)\cdot XnYm+1 - \chi\cdot(2-m)\cdot XnYm\cdot[Ca^{2+}]_i - \delta\cdot b^{m-1}\cdot m\cdot XnYm$$

when n=0, m=0:

$$d(X0Y0)/dt= \beta\cdot X1Y0 - 5\cdot\alpha\cdot X0Y0\cdot[Ca^{2+}]_i + \delta\cdot X0Y1 - 2\cdot\chi\cdot X0Y0\cdot[Ca^{2+}]_i - \gamma1\cdot X0Y0$$

when n=5

$$d(XnYm)/dt= \alpha\cdot(5-n+1)\cdot Xn-1Ym\cdot[Ca^{2+}]_i + \beta\cdot b^{n}\cdot(n+1)\cdot Xn+1Ym - \alpha\cdot(5-n)\cdot XnYm\cdot[Ca^{2+}]_i - \beta\cdot b^{n-1}\cdot n\cdot XnYm + \chi\cdot(2-m+1)\cdot XnYm-1\cdot[Ca^{2+}]_i + \delta\cdot b^{m}\cdot(m+1)\cdot XnYm+1 - \chi\cdot(2-m)\cdot XnYm\cdot[Ca^{2+}]_i - \delta\cdot b^{m-1}\cdot m\cdot XnYm - \gamma2\cdot(XnYm)$$

when m=2

$$d(XnYm)/dt= \alpha\cdot(5-n+1)\cdot Xn-1Ym\cdot[Ca^{2+}]_i + \beta\cdot b^{n}\cdot(n+1)\cdot Xn+1Ym - \alpha\cdot(5-n)\cdot XnYm\cdot[Ca^{2+}]_i - \beta\cdot b^{n-1}\cdot n\cdot XnYm + \chi\cdot(2-m+1)\cdot XnYm-1\cdot[Ca^{2+}]_i + \delta\cdot b^{m}\cdot(m+1)\cdot XnYm+1 - \chi\cdot(2-m)\cdot XnYm\cdot[Ca^{2+}]_i - \delta\cdot b^{m-1}\cdot m\cdot XnYm - \gamma3\cdot(XnYm)$$

The total release within Δt:

$$fuse(t,\Delta t)=[\gamma1\cdot X0Y0+\gamma2\cdot(X5Y0+X5Y1+X5Y2)+\gamma3\cdot(X0Y2+X1Y2+X2Y2+X3Y2+X4Y2+X5Y2)]\cdot\Delta t$$

Where: spontaneous release=$\gamma1\cdot X0Y0\cdot\Delta t$

synchronized release=$\gamma2\cdot(X5Y0+X5Y1+X5Y2)\cdot\Delta t$

asynchronized release=$\gamma3\cdot(X0Y2+X1Y2+X2Y2+X3Y2+X4Y2+X5Y2)\cdot\Delta t$

Miscellaneous

Immunofluorescence labeling and immunoblotting experiments were performed essentially as described[19]. All statistical analyses were performed using Student's t-test.

Supplementary Material

Refer to Web version on PubMed Central for supplementary material.

Acknowledgments

We thank I. Kornblum, A. Roth, L. Fan, and J. Mitchell for excellent technical assistance, and J. Bollmann, X. Lou, and R. Schneggenburger for advice. This study was supported by a grant from NARSAD (to J.S.) and by The University of Texas M. D. Anderson Cancer Center Physician Scientist Program (R.A.).

REFERENCES

1. Meinrenken CJ, Borst JG, Sakmann B. Local routes revisited: the space and time dependence of the Ca^{2+} signal for phasic transmitter release at the rat calyx of Held. J. Physiol. 2003; 547:665–689. [PubMed: 12562955]
2. Schneggenburger R, Neher E. Presynaptic calcium and control of vesicle fusion. Curr. Opin. Neurobiol. 2005; 15:266–274. [PubMed: 15919191]
3. Atluri PP, Regehr WG. Delayed release of neurotransmitter from cerebellar granule cells. J. Neurosci. 1998; 18:8214–8227. [PubMed: 9763467]
4. Lu T, Trussell LO. Inhibitory transmission mediated by asynchronous transmitter release. Neuron. 2000; 26:683–694. [PubMed: 10896163]
5. Hagler DJ Jr. Goda Y. Properties of synchronous and asynchronous release during pulse train depression in cultured hippocampal neurons. J. Neurophysiol. 2001; 85:2324–2334. [PubMed: 11387379]
6. Otsu Y, Shahrezaei V, Li B, Raymond LA, Delaney KR, Murphy TH. Competition between phasic and asynchronous release for recovered synaptic vesicles at developing hippocampal autaptic synapses. J. Neurosci. 2004; 24:420–433. [PubMed: 14724240]

7. Hefft S, Jonas P. Asynchronous GABA release generates long-lasting inhibition at a hippocampal interneuron-principal neuron synapse. Nat. Neurosci. 2005; 8:1319–1328. [PubMed: 16158066]
8. Forsythe ID. Direct patch recording from identified presynaptic terminals mediating glutamatergic EPSCs in the rat CNS, in vitro. J. Physiol. 1994; 479:381–387. [PubMed: 7837096]
9. Borst JG, Sakmann B. Calcium influx and transmitter release in a fast CNS synapse. Nature. 1996; 383:431–434. [PubMed: 8837774]
10. Sun JY, Wu LG. Fast kinetics of exocytosis revealed by simultaneous measurements of presynaptic capacitance and postsynaptic currents at a central synapse. Neuron. 2001; 30:171–182. [PubMed: 11343653]
11. Schneggenburger R, Neher E. Intracellular calcium dependence of transmitter release rates at a fast central synapse. Nature. 2000; 406:889–893. [PubMed: 10972290]
12. Bollmann JH, Sakmann B, Borst JG. Calcium sensitivity of glutamate release in a calyx-type terminal. Science. 2000; 289:953–957. [PubMed: 10937999]
13. Geppert M, Goda Y, Hammer RE, Li C, Rosahl TW, Stevens CF, Südhof TC. Synaptotagmin I: a major Ca^{2+} sensor for transmitter release at a central synapse. Cell. 1994; 79:717–727. [PubMed: 7954835]
14. Fernandez-Chacon R, Königstorffer, Gerber SH, Garcia J, Matos MF, Stevens CF, Brose N, Rizo J, Rosenmund C, Südhof TC. Synaptotagmin I functions as a Ca^{2+}-regulator of release probability. Nature. 2001; 410:41–49. [PubMed: 11242035]
15. Stevens CF, Sullivan JM. The synaptotagmin C_2A domain is part of the calcium sensor controlling fast synaptic transmission. Neuron. 2003; 39:299–308. [PubMed: 12873386]
16. Nagy G, Kim JH, Pang ZP, Matti U, Rettig J, Südhof TC, Sørensen JB. Different effects on fast exocytosis induced by synaptotagmin 1 and 2 isoforms and abundance, but not by phosphorylation. J. Neurosci. 2006; 26:632–643. [PubMed: 16407561]
17. Pang ZP, Melicoff E, Padgett D, Liu Y, Teich AF, Dickey BF, Lin W, Adachi R, Südhof TC. Synaptotagmin-2 is essential for survival and contributes to Ca^{2+} triggering of neurotransmitter release in central and neuromuscular synapses. J. Neurosci. 2006; 26:13493–13504. [PubMed: 17192432]
18. Xu J, Mashimo T, Südhof TC. Synaptotagmin-1, -2, and -9: Ca^{2+}-sensors for fast release that specify distinct presynaptic properties in subsets of neurons. Neuron. 2007; 54:801–812. [PubMed: 17553427]
19. Pang ZP, Sun J, Rizo J, Maximov A, Südhof TC. Genetic analysis of synaptotagmin 2 in spontaneous and Ca^{2+}-triggered neurotransmitter release. EMBO J. 2006; 25:2039–2050. [PubMed: 16642042]
20. Goda Y, Stevens CF. Two components of transmitter release at a central synapse. Proc. Natl. Acad. Sci. U. S. A. 1994; 91:12942–12946. [PubMed: 7809151]
21. Ravin R, Spira ME, Parnas H, Parnas I. Simultaneous measurement of intracellular Ca^{2+} and asynchronous transmitter release from the same crayfish bouton. J. Physiol. 1997; 501:251–262. [PubMed: 9192298]
22. Maximov A, Südhof TC. Autonomous Function of Synaptotagmin 1 in Triggering Asynchronous Release Independent of Asynchronous Release. Neuron. 2005; 48:547–554. [PubMed: 16301172]
23. Chuhma N, Ohmori H. Role of Ca^{2+} in the synchronization of transmitter release at calyceal synapses in the auditory system of rat. J. Neurophysiol. 2002; 87:222–228. [PubMed: 11784744]
24. Schneggenburger R, Forsythe ID. The calyx of Held. Cell Tissue Res. 2006; 326:311–337. [PubMed: 16896951]
25. Lou X, Scheuss V, Schneggenburger R. Allosteric modulation of the presynaptic Ca^{2+} sensor for vesicle fusion. Nature. 2005; 435:497–501. [PubMed: 15917809]
26. Iwasaki S, Takahashi T. Developmental changes in calcium channel types mediating synaptic transmission in rat auditory brainstem. J. Physiol. 1998; 509:419–423. [PubMed: 9575291]
27. Wu LG, Westenbroek RE, Borst JG, Catterall WA, Sakmann B. Calcium channel types with distinct presynaptic localization couple differentially to transmitter release in single calyx-type synapses. J. Neurosci. 1999; 19:726–736. [PubMed: 9880593]

28. Leveque C, el Far O, Martin-Moutot N, Sato K, Kato R, Takahashi M, Seagar MJ. Purification of the N-type calcium channel associated with syntaxin and synaptotagmin. A complex implicated in synaptic vesicle exocytosis. J. Biol. Chem. 1994; 269:6306–6312. [PubMed: 8119979]
29. Charvin N, L'eveque C, Walker D, Berton F, Raymond C, Kataoka M, Shoji-Kasai Y, Takahashi M, De Waard M, Seagar MJ. Direct interaction of the calcium sensor protein synaptotagmin I with a cytoplasmic domain of the alpha1A subunit of the P/Q-type calcium channel. EMBO J. 1997; 16:4591–4596. [PubMed: 9303303]
30. Zhong H, Yokoyama CT, Scheuer T, Catterall WA. Reciprocal regulation of P/Q-type Ca^{2+} channels by SNAP-25, syntaxin and synaptotagmin. Nat. Neurosci. 1999; 2:939–941. [PubMed: 10526329]
31. Sakaba T, Neher E. Quantitative relationship between transmitter release and calcium current at the calyx of held synapse. J. Neurosci. 2001; 21:462–476. [PubMed: 11160426]
32. Stevens CF, Wesseling JF. Activity-dependent modulation of the rate at which synaptic vesicles become available to undergo exocytosis. Neuron. 1998; 21:415–424. [PubMed: 9728922]
33. Mulkey RM, Zucker RS. Action potentials must admit calcium to evoke transmitter release. Nature. 1991; 350:153–155. [PubMed: 1672444]
34. Heidelberger R, Heinemann C, Neher E, Matthews G. Calcium dependence of the rate of exocytosis in a synaptic terminal. Nature. 1994; 371:513–515. [PubMed: 7935764]
35. Awatramani GB, Price GD, Trussell LO. Modulation of transmitter release by presynaptic resting potential and background calcium levels. Neuron. 2005; 48:109–121. [PubMed: 16202712]
36. Taschenberger H, Scheuss V, Neher E. Release kinetics, quantal parameters and their modulation during short-term depression at a developing synapse in the rat CNS. J. Physiol. 2005; 568:513–537. [PubMed: 16096340]
37. Wadel K, Neher E, Sakaba T. The coupling between synaptic vesicles and Ca^{2+} channels determines fast neurontransmitter release. Neuron. 2007; 53:563–575. [PubMed: 17296557]
38. Wölfel M, Lou X, Schneggenburger R. A mechanism intrinsic to the vesicle fusion machinery determines fast and slow transmitter release at a large CAN synapse. J. Neurosci. 2007; 27:3198–3120. [PubMed: 17376981]
39. Trommershauser J, Schneggenburger R, Zippelius A, Neher E. Heterogeneous presynaptic release probabilities: functional relevance for short-term plasticity. Biophys. J. 2003; 84:1563–1579. [PubMed: 12609861]
40. Kushmerick C, Renden R, von Gersdorff H. Physiological temperatures reduce the rate of vesicle pool depletion and short-term depression via an acceleration of vesicle recruitment. J. Neurosci. 2006; 26:1366–1377. [PubMed: 16452660]
41. Bollmann JH, Sakmann B. Control of synaptic strength and timing by the release-site Ca^{2+} signal. Nat. Neurosci. 2005; 8:426–434. [PubMed: 15750590]
42. Sun J, Bronk P, Liu X, Han W, Südhof TC. Synapsins regulate use-dependent synaptic plasticity in the calyx of Held by a Ca^{2+}/calmodulin-dependent pathway. Proc. Natl. Acad. Sci. U. S. A. 2006; 103:2880–2885. [PubMed: 16481620]
43. Grynkiewicz G, Poenie M, Tsien RY. A new generation of Ca^{2+} indicators with greatly improved fluorescence properties. J. Biol. Chem. 1985; 260:3440–3450. [PubMed: 3838314]

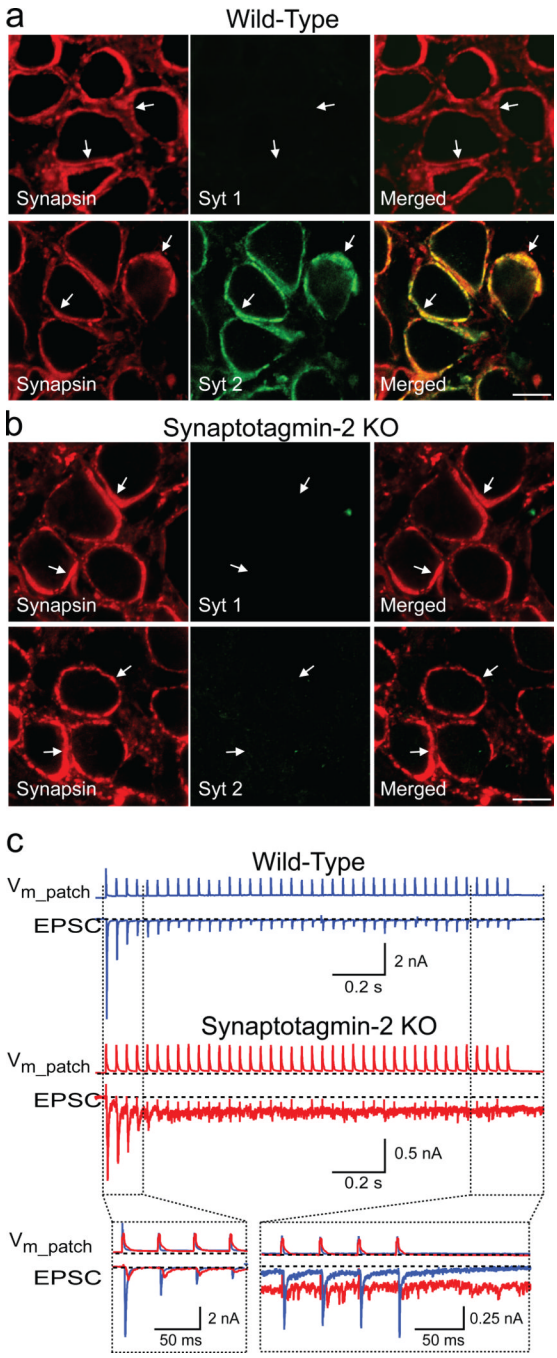

Figure 1. Calyx synapses in synaptotagmin-2 deficient mice

a. and **b**. Immunofluorescence analysis of brainstem sections from wild-type (a) and synaptotagmin-2 deficient mice (b) at P11 with antibodies to synapsins (red; left panels) and synaptotagmin-1 or -2 (green; middle panels). Merged images are shown on the right with coincident staining in yellow (scale bar = 10 μm, applies to all panels; arrows = synapses; Syt 1 and 2 = synaptotagmin-1 and -2 (see also Suppl. Fig. 2).

c. EPSCs recorded in response to 25 Hz action potential stimulation induced by a cell-attached presynaptic pipette (V_{m_patch} = extracellular voltage in the patched area). The insert at the bottom shows a superposition of wild-type and mutant traces.

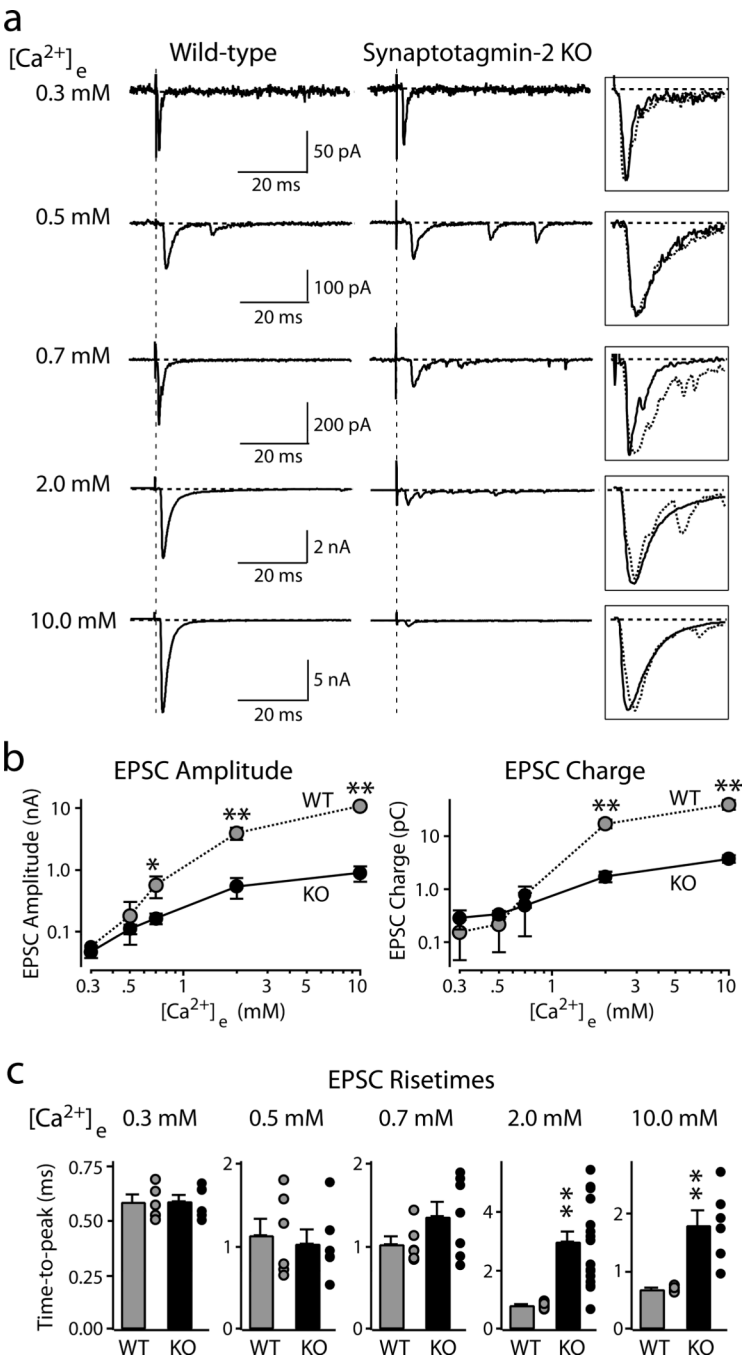

Figure 2. Synaptic transmission evoked by isolated action potentials

Postsynaptic voltage-clamp recordings of ESPCs evoked by afferent fiber stimulation in wild-type (left) and synaptotagmin-2 deficient calyx synapses (right) at the indicated $[Ca^{2+}]_e$ in the presence of 50 μM AP-5.

a. Representative EPSCs. Boxed traces on right display scaled superimposed EPSCs to illustrate EPSC kinetics.

b. Double-logarithmic plots of EPSC amplitudes (left panel) or EPSC charge transfer (right panel) as a function of $[Ca^{2+}]_e$ (means ± SEMs; number of recordings/$[Ca^{2+}]_e$: WT, 5/0.3

mM, 6/0.5 mM, 6/0.7 mM, 14/2 mM, 5/10 mM; KO, 6/0.3 mM, 6/0.5 mM, 7/0.7 mM, 17/2 mM, 6/10 mM).

c. Summary graphs of the time-to-peak of EPSCs recorded for the indicated $[Ca^{2+}]_e$. For each Ca^{2+}-concentration, the bar depicts means ± SEMs; dots next to the bar exhibit individual data points (*=p<0.05; **=p<0.01; Student's t-test).

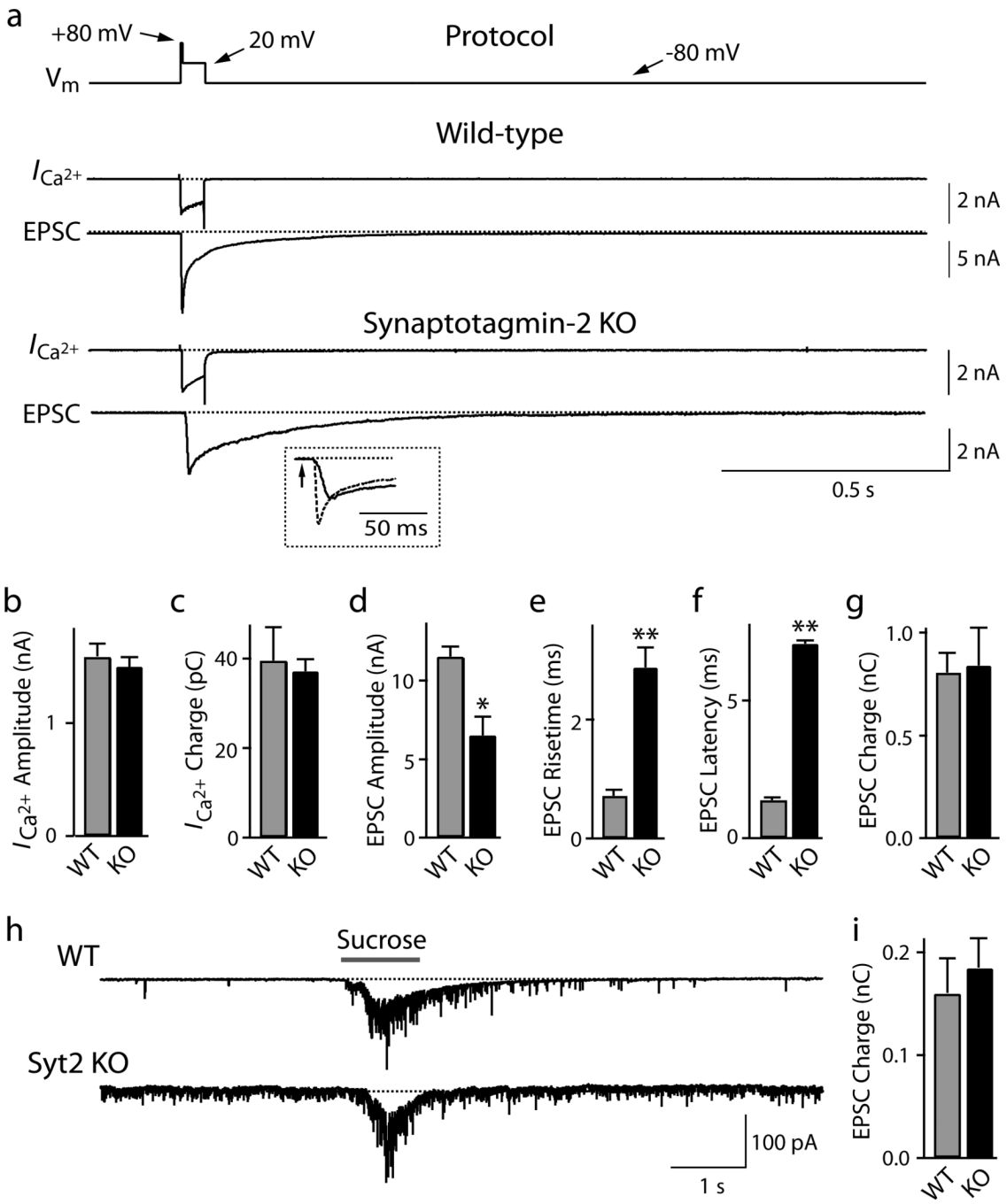

Figure 3. RRP size, Ca^{2+}-currents, and release kinetics in synaptotagmin-2 deficient calyx synapses

a. Experimental protocol involving a 4 ms predepolarization followed by a 50 ms depolarization (top line), and representative traces of presynaptic Ca^{2+}-currents (I_{Ca}) and postsynaptic EPSCs (bottom traces). The inset displays an expansion of the initial phase of the EPSCs from wild-type (dotted line) and synaptotagmin-2 deficient terminals (continuous line). Experiments were performed by simultaneous pre- and postsynaptic voltage-clamp recordings in calyx terminals at P7–P9 in 0.1 μM tetrodotoxin, 0.1 mM cyclothiazide, 1 mM kynurenic acid, and 50 μM D-AP5.

b.– **g.** Ca^{2+}-current amplitudes (b), Ca^{2+}-current electrical charge transfer (c, integrated over 100 ms), EPSC amplitudes (d), EPSC rise times (e; 20–80%), EPSC latencies (f; from onset of Ca^{2+}-current to 10% of the EPSC), and EPSC charge transfer (g; integrated over 2 s) induced by sustained presynaptic depolarization. Data shown are means ± SEMs (WT: n=12; KO: n=14).

h. and **i**. Representative traces (h) and summary graphs of the electric charge transfer (i; integrated over 5 s) of synaptic responses induced by 1 s applications of 2 M sucrose via a glass pipette positioned ~5 μm from the calyx (means ± SEMs; WT: n=10; KO: n=11).

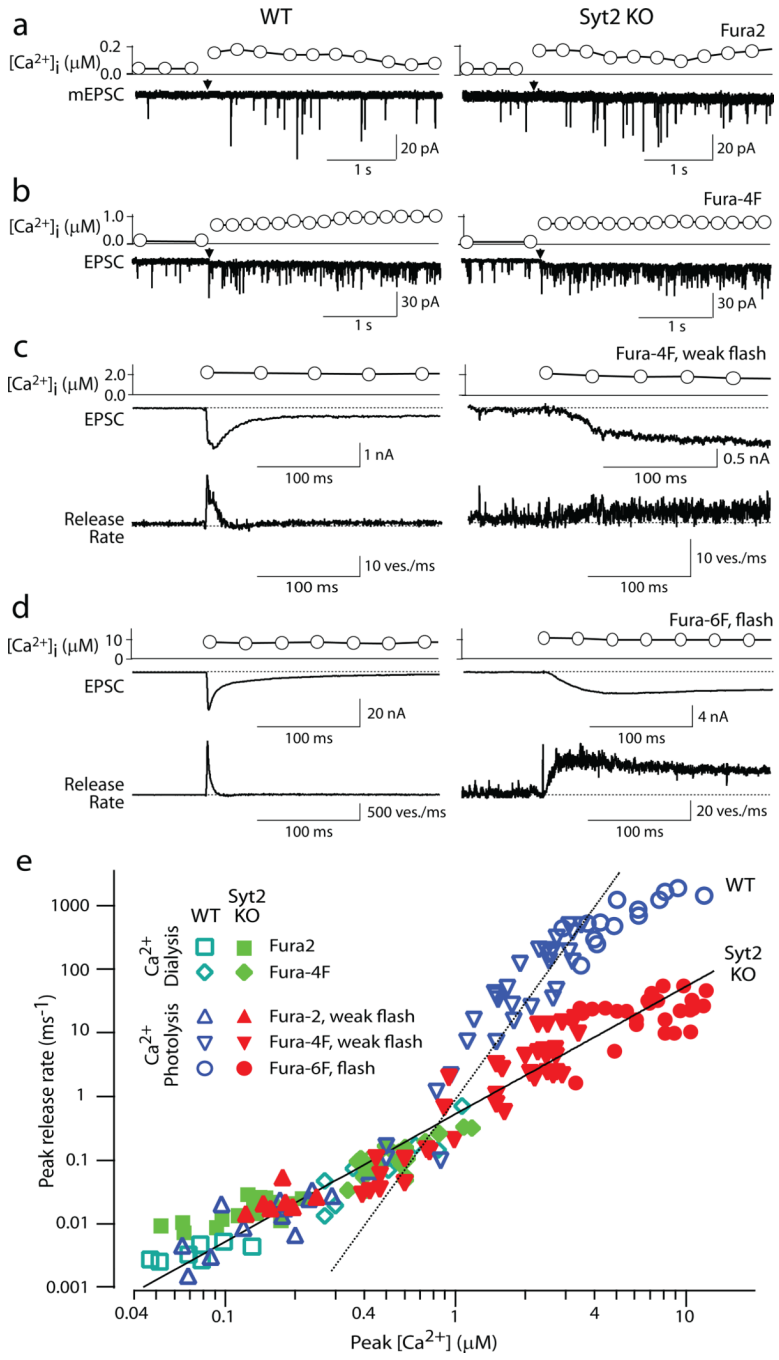

Figure 4. Relationship between peak vesicular release rates and $[Ca^{2+}]_i$ in calyx terminals

EPSC were recorded in calyx synapses in the double-patch configuration at P7~P9 in the presence of 0.1 μM tetrodotoxin, 0.1 mM cyclothiazide, 1 mM kynurenic acid, and 50 μM D-AP5. Presynaptic $[Ca^{2+}]_i$ increases were achieved by photolysis of caged Ca^{2+} dialyzed into the terminal, or by dialysis of buffered Ca^{2+} at low $[Ca^{2+}]$. $[Ca^{2+}]_i$ was monitored optically using three different Ca^{2+}-sensitive dyes as indicated (for *in situ* calibration of $[Ca^{2+}]_i$, see Suppl. Materials).

a–d. Representative experiments in wild-type (left panels) and synaptotagmin-2 deficient calyces (right panels) at four characteristic Ca^{2+}-concentrations; the Ca^{2+}-indicator dyes

used are shown on the right. Panels c and d also display the vesicle release rate as calculated by EPSC deconvolutions.

e. Summary graph of EPSC peak release rates and $[Ca^{2+}]_i$ (n=78 for wild-type [open symbols], 106 for synaptotagmin-2 deficient terminals [filled symbols]; green symbols represent the data obtained by dialysis of Ca^{2+}-buffers into the terminals via the patch pipette). The dashed line represents a fit of a 5^{th} power function to the data from wild-type terminals at $[Ca^{2+}]_i$ = >1μM ($y=0.90 \cdot x^5$); the solid line a 2^{nd} power function to the data from mutant terminals ($y=0.54 \cdot x^2$); note that the solid line also fits the wild-type responses at low $[Ca^{2+}]_i$.

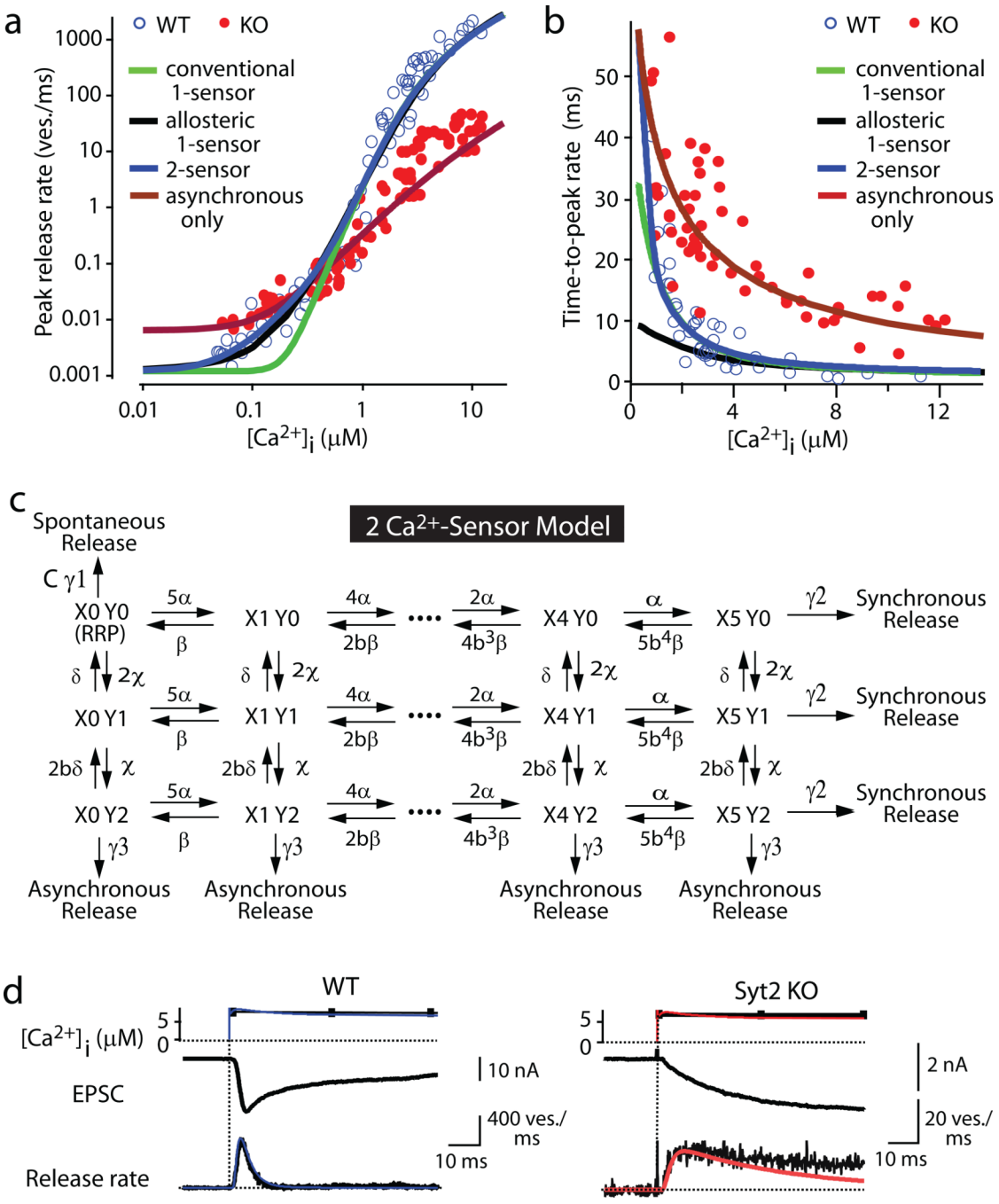

Figure 5. A two Ca^{2+}-sensor model for neurotransmitter release

a. and **b.** Fits of the Ca^{2+}-photolysis data from wild-type and synaptotagmin-2 deficient calyces for the peak release rate (a) and time-to-peak rate (b) to the conventional 1-sensor model[11,12], the allosteric 1-sensor model[25], the 2-sensor model, and the 2-sensor model with inactivation of the synchronous Ca^{2+}-sensor (see Suppl. Materials and Suppl. Figs. 10–13 for details; RRP is set to 3000 vesicles[11,12]).

c. Reaction scheme. $\gamma 1$, $\gamma 2$, $\gamma 3$ = rates of spontaneous, synchronous, and asynchronous release, respectively (defined as the fraction of the RRP released per second); α and β, and χ and $\delta = k_{on}$ and k_{off} for Ca^{2+}-action for synchronous and asynchronous release,

respectively; X0-X5 and Y0-Y2 = Ca^{2+}-binding states of the Ca^{2+}-sensor for synchronous (X) and asynchronous release (Y), respectively (note that X0Y0 = RRP); b = cooperativity factor[11,12]. The curve fitting parameters were (only $\gamma 1$ differs between wild-type and KO): α=1.53 10^8 $M^{-1}s^{-1}$, β=5800 s^{-1}, b=0.25; χ=2.94 10^6 $M^{-1}s^{-1}$, δ=130 s^{-1}, $\gamma 1$=0.417 10^{-3} ms^{-1} in wild-type and 2.23 10^{-3} s^{-1} in KO; $\gamma 2$= 6,000 s^{-1}; $\gamma 3$= 6,000 s^{-1}. $\gamma 1$ was measured experimentally, b and $\gamma 2$ were from ref. 11, and $\gamma 3$ assumed to be equal to $\gamma 2$ based on the postulate that Ca^{2+}-binding to the asynchronous and synchronous release Ca^{2+}-sensors will trigger the same release rates since both empty the entire RRP. **d.** Local $[Ca^{2+}]_i$ signal predicted by the Ca^{2+}-relaxation model (Suppl. Fig. 12) and transmitter release rates predicted by the two Ca^{2+}-sensor model in wild-type (left) and synaptotagmin-2 KO calyces (right). Top panels: measured and predicted $[Ca^{2+}]_i$ (black and blue or red, respectively); middle panels: recorded EPSCs; lower panels: vesicular release rates deconvoluted from EPSCs (black), and predicted by the model (blue or red).